Available online at www.sciencedirect.com
ScienceDirect
International Journal of Thermal Sciences 48 (2009) 502–513
International Journal of Thermal Sciences
www.elsevier.com/locate/ijts

A three-dimensional inverse geometry problem in identifying irregular boundary configurations

Cheng-Hung Huang *, Meng-Ting Chaing

Department of Systems and Naval Mechatronic Engineering, National Cheng Kung University, Tainan, Taiwan, ROC

Received 24 December 2007; received in revised form 15 May 2008; accepted 15 May 2008

Available online 17 June 2008

Abstract

A three-dimensional inverse geometry problem (shape identification problem) in determining the unknown irregular surface configurations by utilizing the conjugate gradient method (CGM) and a general purpose commercial code CFD-RC is successfully developed and examined in this study based on the simulated measured temperature distributions on the bottom surface by infrared thermography. Results obtained by using the technique of CGM to solve the inverse geometry problem are justified based on the numerical experiments. Three test cases are performed to test the validity of the present algorithm by using different types of surface shapes, initial guess and measurement errors. Results show that excellent estimations on the unknown surface geometry can be obtained with any arbitrary initial guesses.

Keywords: Inverse geometry problem; Irregular boundary configurations estimation

1. Introduction

The applications of Inverse Heat Conduction Problems (IHCP) can be found in several engineering fields in estimating thermal quantities, such as the determination of unknown heat fluxes [1], thermal properties [2] and heat sources [3], etc., when the geometry of the physical problems under consideration are known. However, when the geometry of the problems is subjected to change and unknown, the technique of Inverse Geometry Problem (IGP) should be used to estimate the position varying domain configurations. Recently, thermal imaging, the application of Inverse Geometry Problem, has become another area of active inverse problem research, and much research has been devoted to infrared scanners and their applications to nondestructive evaluation (NDE) [4] and shape identifications [5]. The approaches taken to solve NDE or shape identification problems are based on either steady or unsteady state response of a body subjected to thermal sources.

For the inverse geometry problem, due to its inherent nature, it requires a complete regeneration of the mesh as the geometry evolves. Moreover, the continuous evolution of the geometry itself poses certain difficulties in arriving at analytical or numerical solutions. For this reason it is necessary to use an efficient technique that can handle the problems with irregular surface geometry, especially in 3-D applications.

The inverse geometry problems, including the cavity or shape estimation, have been solved by a variety of numerical methods [6–10]. Huang and his co-workers have utilized the conjugate gradient method (CGM) and boundary element technique to the inverse geometry problems and have published a series of relevant papers. Huang and Chao [11] first derived the formulations for determining the unknown irregular boundary configurations for a 2-D steady-state shape identification problem with CGM. Based on the algorithm developed in [11], Huang and Tsai [12] extended the algorithm to a transient inverse geometry problem in identifying the unknown irregular boundary configurations from external measurements. Huang et al. [13] have developed a new algorithm for two-dimensional multiple cavities estimations where the search directions are not confined, i.e. the unknown parameters become x- and y-coordinates. Huang and Chen [14] extended the similar algorithm to a multiple region domain in estimating the time and space varying outer boundary configurations. Huang and

* Corresponding author.
E-mail address: chhuang@mail.ncku.edu.tw (C.-H. Huang).

1290-0729/$ – see front matter
doi:10.1016/j.ijthermalsci.2008.05.007

Nomenclature

$f(x, y)$	unknown irregular surface configurations
J	functional defined by Eq. (2)
J'	gradient of functional defined by Eq. (15)
P	direction of descent defined by Eq. (4)
q	heat flux density
$T(x, y, z)$	estimated temperature
T_0	boundary temperature on S_{top}
$\Delta T(x, y, z)$	sensitivity function defined by Eq. (6)
$Y(S_{\text{bottom}})$	measured temperatures

Greeks

β	search step size
γ	conjugate coefficient
Ω	computational domain
$\lambda(x, y, z)$	Lagrange multiplier defined by Eq. (12)
$\delta(\cdot)$	Dirac delta function
ω	random number
ε	convergence criterion
σ	standard deviation of the measurement errors

Superscript

n	iteration index

Shih [15] applied the technique to a shape identification problem in estimating simultaneously two interfacial configurations in a multiple region domain.

It should be noted that the above references are all 2-D inverse geometry problems; the 3-D inverse geometry problems are still very limited in the literatures. Recently Divo et al. [16] have used a singular superposition technique and the genetic algorithm for detecting the unknown cavity in a 3-D inverse geometry problem. In their study the shape of a 3-D cavity is only a sphere, not an arbitrary shape, and the convergent speed for the genetic algorithm may also be slow.

The commercial code CFD-RC [17] is available for solving fluid dynamic and heat transfer problems. The advantage of calling CFD-RC as a subroutine in the present inverse calculation lies in that its auto mesh function enables the handling of this moving boundary problem. The "moving boundary problem" implies actually that the boundary configurations are subjected to change in each iterative process. This code can be used to calculate many practical but difficult direct thermal problems.

If one can devise an inverse algorithm, which has the ability to communicate with the commercial code by means of data transportation, a generalized 3-D inverse geometry problem can thus be established. The objective of the present study is to extend the previous studies on the inverse geometry problems by the authors [11–15] and to utilize the CFD-RC code as the subroutine in solving the 3-D inverse geometry problem by CGM.

The CGM is also called an iterative regularization method, which means the regularization procedure is performed during the iterative processes and thus the determination of optimal regularization conditions is not needed. The conjugate gradient method derives from the perturbation principles and transforms the inverse geometry problem to the solution of three problems, namely, the direct, sensitivity and the adjoint problem.

These three problems are solved by CFD-RC and the calculated values are used in CGM for inverse calculations. The bridge between CFD-RC and CGM is the INPUT/OUTPUT files. Those files should be arranged such that their format can be recognized by CFD-RC and CGM. A sequence of forward steady-state heat conduction problems is solved by CFD-RC in an effort to update the boundary geometry by minimizing a residual measuring the difference between estimated and measured temperatures at the temperature extracting locations under the present algorithm.

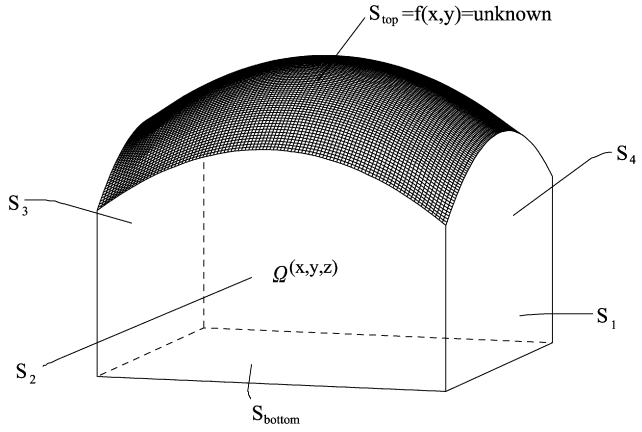

Fig. 1. Geometry and coordinates.

Finally the inverse solutions for this study with three different irregular surface geometries will be illustrated to show the validity of using CGM in the present 3-D inverse geometry problem.

2. The direct problem

To illustrate the methodology for developing expressions for use in determining unknown boundary geometry in a homogeneous medium, we consider the following three-dimensional steady state inverse heat conduction problem. For a domain Ω, the boundary conditions on four side surfaces S_1, S_2, S_3 and S_4 are all assumed insulated, on the bottom surface S_{bottom}, a constant heat flux q is taken away from the boundary by cooling while the boundary condition on the top surface S_{top}, $z = f(x, y)$, maintains at an uniform temperature T_0. Fig. 1 shows the geometry and the coordinates for the three-dimensional physical problem considered here. The mathematical formulation of this steady-state heat conduction problem in dimensional form is given by:

$$\frac{\partial^2 T}{\partial x^2}+\frac{\partial^2 T}{\partial y^2}+\frac{\partial^2 T}{\partial z^2}=0 \quad \text{in } \Omega \tag{1a}$$

$$\frac{\partial T}{\partial x}=0 \quad \text{on } S_1 \tag{1b}$$

$$\frac{\partial T}{\partial x}=0 \quad \text{on } S_2 \tag{1c}$$

$$\frac{\partial T}{\partial y}=0 \quad \text{on } S_3 \tag{1d}$$

$$\frac{\partial T}{\partial y}=0 \quad \text{on } S_4 \tag{1e}$$

$$k\frac{\partial T}{\partial z}=q \quad \text{on } S_{\text{bottom}} \tag{1f}$$

$$T=T_0 \quad \text{on } S_{\text{top}},\ z=f(x,y) \tag{1g}$$

The above problem is solved by the following the commercial package CFD-RC for the reason that it has the function of auto mesh.

The direct problem considered here is concerned with the determination of the medium temperature when the boundary geometry $z=f(x,y)$ and the boundary conditions at all boundaries are known.

3. The inverse geometry problem

For the inverse geometry problem, the boundary geometry $z=f(x,y)$ is regarded as being unknown, but everything else in Eq. (1) is known. In addition, simulated temperature readings taken by infrared scanners on the bottom surface S_{bottom} are considered available. In this work no real measured temperatures were utilized, instead, the simulated values of measured temperatures on S_{bottom} are generated by using the exact geometry of the top surface in the solution of direct problem. Then try to retrieve the geometry of the top surface by using simulated measured temperatures on S_{bottom} and the technique of the CGM.

Referring to Fig. 1, let the temperature reading taken by infrared scanners on the bottom surface S_{bottom} be denoted by $\mathbf{Y}(S_{\text{bottom}}) \equiv Y(x_m, y_m) \equiv Y_m(S_{\text{bottom}})$, $m=1$ to M, where M represents the number of measured temperature extracting points. We note that the measured temperature $Y_m(S_{\text{bottom}})$ contain measurement errors. Then the shape identification problem can be stated as follows: by utilizing the above mentioned measured temperature data $Y_m(S_{\text{bottom}})$, estimate the unknown geometry of the top surface, $z=f(x,y)$.

The solution of the present inverse geometry problem is to be obtained in such a way that the following functional is minimized:

$$J\big[f(x,y)\big]=\sum_{m=1}^{M}\big[T_m(S_{\text{bottom}})-Y_m(S_{\text{bottom}})\big]^2 = \int_{S_{\text{bottom}}}(T-Y)^2\delta(x-x_m)\delta(y-y_m)\,dS_{\text{bottom}} \tag{2}$$

where $\delta(x-x_m)$ and $\delta(y-y_m)$ are the Dirac delta function and T_m are the estimated or computed temperatures on the measured positions (x_m, y_m) on S_{bottom}. These quantities are determined from the solution of the direct problem given previously by using estimated boundary geometry for the exact $f(x,y)$.

4. Conjugate gradient method for minimization

The Conjugate Gradient Method itself may not ensure the global minimum; however, if the objective function is properly defined and in a quadratic form, like the definition in Eq. (2), the global minimum for this objective function is guaranteed.

The following iterative process based on the conjugate gradient method [11–15] is now used for the estimation of unknown boundary geometry $f(x,y)$ by minimizing the functional $J[f(x,y)]$

$$f^{n+1}(x,y)=f^n(x,y)-\beta^n P^n(x,y) \quad \text{for } n=0,1,2,\ldots \tag{3}$$

where β^n is the search step size in going from iteration n to iteration $n+1$, and $P^n(x,y)$ is the direction of descent (i.e. search direction) given by

$$P^n(x,y)=J'^n(x,y)+\gamma^n P^{n-1}(x,y) \tag{4}$$

which is a conjugation of the gradient direction $J'^n(x,y)$ at iteration n and the direction of descent $P^{n-1}(x,y)$ at iteration $n-1$. The conjugate coefficient is determined from

$$\gamma^n=\frac{\int_{S_{\text{top}}}(J'^n)^2\,dS_{\text{top}}}{\int_{S_{\text{top}}}(J'^{n-1})^2\,dS_{\text{top}}} \quad \text{with } \gamma^0=0 \tag{5}$$

We note that when $\gamma^n=0$ for any n, in Eq. (4), the direction of descent $P^n(x,y)$ becomes the gradient direction, i.e. the "Steepest descent" method is obtained. The convergence of the above iterative procedure in minimizing the functional J is guaranteed in [18].

To perform the iterations according to Eqs. (3), we need to compute the step size β^n and the gradient of the functional $J'^n(x,y)$. In order to develop expressions for the determination of these two quantities, a "sensitivity problem" and an "adjoint problem" need to be constructed as described below.

5. Sensitivity problem and search step size

The sensitivity problem is obtained from the original direct problem defined by Eq. (1) in the following manner: It is assumed that when $z=f(x,y)$ undergoes a variation Δz (or $\Delta f(x,y)$) in z direction only with both x and y fixed, $T(x,y,z)$ is perturbed by $T+\Delta T$. Then replacing in the direct problem f by $f+\Delta f$ and T by $T+\Delta T$, subtracting the direct problem from the resulting expressions and neglecting the second-order terms, the following sensitivity problem for determining the sensitivity function ΔT is obtained.

$$\frac{\partial^2 \Delta T}{\partial x^2}+\frac{\partial^2 \Delta T}{\partial y^2}+\frac{\partial^2 \Delta T}{\partial z^2}=0 \quad \text{in } \Omega \tag{6a}$$

$$\frac{\partial \Delta T}{\partial x}=0 \quad \text{on } S_1 \tag{6b}$$

$$\frac{\partial \Delta T}{\partial x}=0 \quad \text{on } S_2 \tag{6c}$$

$$\frac{\partial \Delta T}{\partial y}=0 \quad \text{on } S_3 \tag{6d}$$

$$\frac{\partial \Delta T}{\partial y} = 0 \quad \text{on } S_4 \tag{6e}$$

$$\frac{\partial \Delta T}{\partial z} = 0 \quad \text{on } S_{\text{bottom}} \tag{6f}$$

$$\Delta T = \Delta f \frac{\partial T}{\partial z} \quad \text{on } S_{\text{top}},\ z = f(x, y) \tag{6g}$$

The commercial package CFD-RC is used to solve the above sensitivity problem.

The functional $J(f^{n+1})$ for iteration $n+1$ is obtained by rewriting Eq. (2) as

$$J(f^{n+1}) = \int_{S_{\text{bottom}}} \left[T(x, y, z; f^n - \beta^n P^n) - Y\right]^2 \times \delta(x - x_m)\delta(y - y_m)\, dS_{\text{bottom}} \tag{7}$$

where we have replaced $f^{n+1}(x, y)$ by the expression given by Eq. (3). If temperature $T(x, y, z; f^n - \beta^n P^n)$ is linearized by a Taylor expansion, Eq. (7) takes the form

$$J(f^{n+1}) = \int_{S_{\text{bottom}}} \left[T(x, y, z; f^n) - \beta^n \Delta T(x, y, z; P^n) - Y\right]^2 \times \delta(x - x_m)\delta(y - y_m)\, dS_{\text{bottom}} \tag{8}$$

where $T(x, y, x; f^n)$ is the solution of the direct problem by using the estimated $f^n(x, y)$ for exact $f(x, y)$ on the top surface S_{top}. The sensitivity functions $\Delta T(x, y, x; P^n)$ are taken as the solutions of problem (6) at the measured positions (x_m, y_m) on S_{bottom} by letting $\Delta f = P^n$. The search step size β^n is determined by minimizing the functional given by Eq. (8) with respect to β^n. The following expression results:

$$\beta^n = \frac{\int_{S_{\text{bottom}}} (T - Y)\Delta T \delta(x - x_m)\delta(y - y_m)\, dS_{\text{bottom}}}{\int_{S_{\text{bottom}}} (\Delta T)^2 \delta(x - x_m)\delta(y - y_m)\, dS_{\text{bottom}}} \tag{9}$$

6. Adjoint problem and gradient equation

To obtain the adjoint problem, Eq. (1a) is multiplied by the Lagrange multiplier (or adjoint function) $\lambda(x, y, z)$ and the resulting expression is integrated over the correspondent space domain. The result is then added to the right-hand side of Eq. (2) to yield the following expression for the functional $J[f(x, y)]$:

$$J\left[f(x, y)\right] = \int_{S_{\text{bottom}}} (T - Y)^2 \delta(x - x_m)\delta(y - y_m)\, dS_{\text{bottom}} + \int_{x=0}^{L}\int_{y=0}^{L}\int_{z=0}^{f(x,y)} \lambda(x, y, z) \times \left\{\frac{\partial^2 T}{\partial x^2} + \frac{\partial^2 T}{\partial y^2} + \frac{\partial^2 T}{\partial z^2}\right\} dz\, dy\, dx \tag{10}$$

The variation ΔJ is obtained by perturbing f by Δf and T by ΔT in Eq. (10), subtracting the original equation (10) from the resulting expression and neglecting the second-order terms. We thus find

$$\Delta J\left[f(x, y)\right] = \int_{S_{\text{bottom}}} 2[T - Y]\Delta T \delta(x - x_m) \times \delta(y - y_m)\, dS_{\text{bottom}} + \int_{x=0}^{L}\int_{y=0}^{L}\int_{z=0}^{f(x,y)} \lambda(x, y, z) \times \left\{\frac{\partial^2 \Delta T}{\partial x^2} + \frac{\partial^2 \Delta T}{\partial y^2} + \frac{\partial^2 \Delta T}{\partial z^2}\right\} dz\, dy\, dx \tag{11}$$

where $\delta(x - x_m)$ and $\delta(y - y_m)$ are the Dirac delta function and (x_m, y_m), $n = 1$ to M, refer to the temperature extracting points. In Eq. (11), the triple domain integral term is integrated by parts; the boundary conditions of the sensitivity problem given by Eqs. (6b)–(6g) are utilized and then ΔJ is allowed to go to zero. The vanishing of the integrands containing ΔT leads to the following adjoint problem for the determination of $\lambda(x, y, z)$:

$$\frac{\partial^2 \lambda}{\partial x^2} + \frac{\partial^2 \lambda}{\partial y^2} + \frac{\partial^2 \lambda}{\partial z^2} = 0 \quad \text{in } \Omega \tag{12a}$$

$$\frac{\partial \lambda}{\partial x} = 0 \quad \text{on } S_1 \tag{12b}$$

$$\frac{\partial \lambda}{\partial x} = 0 \quad \text{on } S_2 \tag{12c}$$

$$\frac{\partial \lambda}{\partial y} = 0 \quad \text{on } S_3 \tag{12d}$$

$$\frac{\partial \lambda}{\partial y} = 0 \quad \text{on } S_4 \tag{12e}$$

$$\frac{\partial \lambda}{\partial z} = -2(T - Y)\delta(x - x_m)\delta(y - y_m) \quad \text{on } S_{\text{bottom}} \tag{12f}$$

$$\lambda = 0 \quad \text{on } S_{\text{top}},\ z = f(x, y) \tag{12g}$$

The techniques of CFD-RC can be used to solve the above adjoint problem.

Finally, the following integral term is left

$$\Delta J = \int_{S_{\text{top}}} -\left[\frac{\partial \lambda}{\partial z}\frac{\partial T}{\partial z}\right]_{z=f(x,y)} \Delta f(x, y)\, dS_{\text{top}} \tag{13}$$

From definition [1], the functional increment can be presented as

$$\Delta J = \int_{S_{\text{top}}} J'(x, y)\Delta f(x, y)\, dS_{\text{top}} \tag{14}$$

A comparison of Eqs. (13) and (14) leads to the following expression for the gradient of functional $J'(x, y)$ of the functional $J[f(x, y)]$:

$$J'(x, y) = -\left.\frac{\partial \lambda}{\partial z}\frac{\partial T}{\partial z}\right|_{z=f(x,y)} \tag{15}$$

7. Stopping criterion

If the problem contains no measurement errors, the traditional check condition is specified as

$$J\left[f^{n+1}(x, y)\right] < \varepsilon \tag{16}$$

where ε is a small specified number. However, the temperature reading taken by infrared scanners may contain measurement errors. Therefore, it is not expected that the functional equation (2) to be equal to zero at the final iteration step. Following the experience of the authors [1,11–15], the discrepancy principle is utilized as the stopping criterion, i.e. the temperature residuals may be approximated by

$$T(S_{\text{bottom}}) - Y(S_{\text{bottom}}) \approx \sigma \tag{17}$$

where σ is the standard deviation of the temperature measurements, which is assumed to be a constant. Substituting Eq. (17) into Eq. (2), the following expression is obtained for ε:

$$\varepsilon = \sigma^2 M \tag{18}$$

The stopping criterion is given by Eq. (16) with ε determined from Eq. (18).

8. Computational procedure

The computational procedure for the solution of this inverse geometry problem using CGM may be summarized as follows:

Suppose $f^n(x, y)$ is available at iteration n.

Step 1. Solve the direct problem given by Eq. (1) for $T(x, y, z)$.
Step 2. Examine the stopping criterion ε for convergence. Continue if not satisfied.
Step 3. Solve the adjoint problem given by Eq. (12) for $\lambda(x, y, z)$.
Step 4. Compute the gradient of the functional $J'(x, y)$ from Eq. (15).
Step 5. Compute the conjugate coefficient γ^n and direction of descent P^n from Eqs. (5) and (4), respectively.
Step 6. Set $\Delta f(x, y) = P^n(x, y)$, and solve the sensitivity problem given by Eq. (6) for $\Delta T(x, y, z)$.
Step 7. Compute the search step size β^n from Eq. (9).
Step 8. Compute the new estimation for $f^{n+1}(x, y)$ from Eq. (3) and return to step 1.

9. Results and discussions

To illustrate the validity of CGM in identifying irregular boundary configuration $z = f(x, y)$ in a 3-D inverse geometry problem based on the knowledge of the simulated temperature recordings taken by infrared scanners on the bottom surface S_{bottom}, we consider three specific examples where the surface geometry on S_{top}, $z = f(x, y)$, are assumed as three different functions, the first two are the combination of sine and cosine functions and the third one is a step function.

The objective of this article is to show the accuracy of CGM in estimating $f(x, y)$ with no prior information on the functional form of the unknown quantities, which is the so-called function estimation.

In order to compare the results for situations involving random measurement errors, we assume normally distributed uncorrelated errors with zero mean and constant standard deviation. The simulated inexact measurement data $\mathbf{Y}$ can be expressed as

$$\mathbf{Y} = \mathbf{Y}_{\text{dir}} + \omega\sigma \tag{19}$$

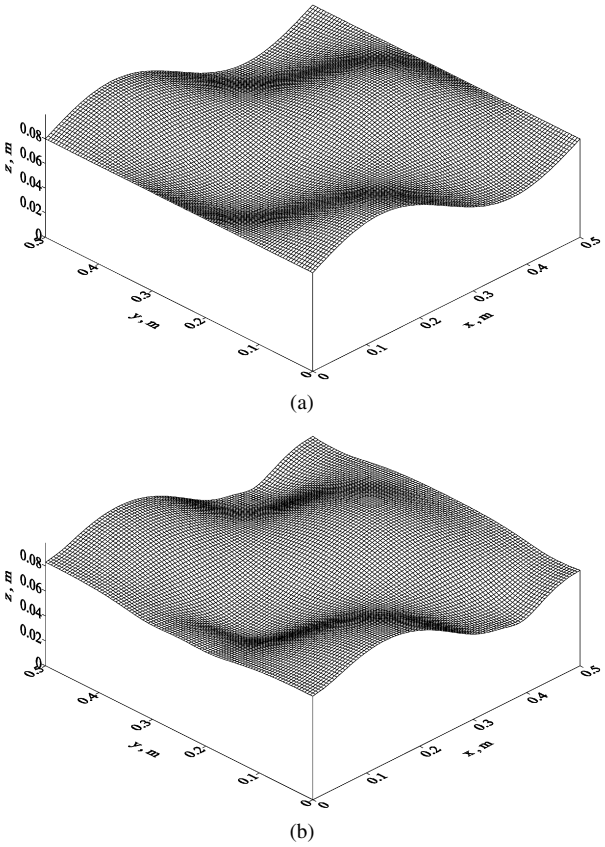

Fig. 2. The (a) exact and (b) estimated surface configurations $f(x, y)$ with $\sigma = 0.0$ and $f(x, y)^0 = 0.05$ m in case 1.

where $\mathbf{Y}_{\text{dir}}$ is the solution of the direct problem with an exact $f(x, y)$; σ is the standard deviation of the measurement error; and ω is a random variable that generated by subroutine DRNNOR of the IMSL [19] and will be within -2.576 to 2.576 for a 99% confidence bounds.

One of the advantages of using the conjugate gradient method is that it does not require a very accurate initial guess of the unknown quantities, this can be verified in the following numerical experiments.

To discuss the effect of grid number on the calculated temperatures for the direct problem, a benchmark problem with L_x (length in x direction) $= L_y$ (length in y direction) $= 0.5$ m, L_z (length in z direction) $= 0.1$ m, $q = -5000\ \text{W/m}^2$ and $T_0 = 200\,^\circ\text{C}$ is considered. The grid number in x, y and z directions are $31 \times 31 \times 11$, $51 \times 51 \times 21$, $71 \times 71 \times 31$ and $111 \times 111 \times 51$, respectively. The case for $111 \times 111 \times 51$ grid system is regarded as the true solution for the benchmark problem.

The relative errors between the true and computed temperatures on S_{bottom} for $31 \times 31 \times 11$, $51 \times 51 \times 21$ and $71 \times 71 \times 31$ grid system are calculated as 6.32%, 0.98% and 0.73%, respectively. It is obvious that $51 \times 51 \times 21$ grid system is accurate enough for the present numerical solution.

Based on the above stated grid independent test, in all the test cases considered here we have chosen $L_x = L_y = 0.5$ m and the spacing in numerical computations is taken as $\Delta x = \Delta y =$

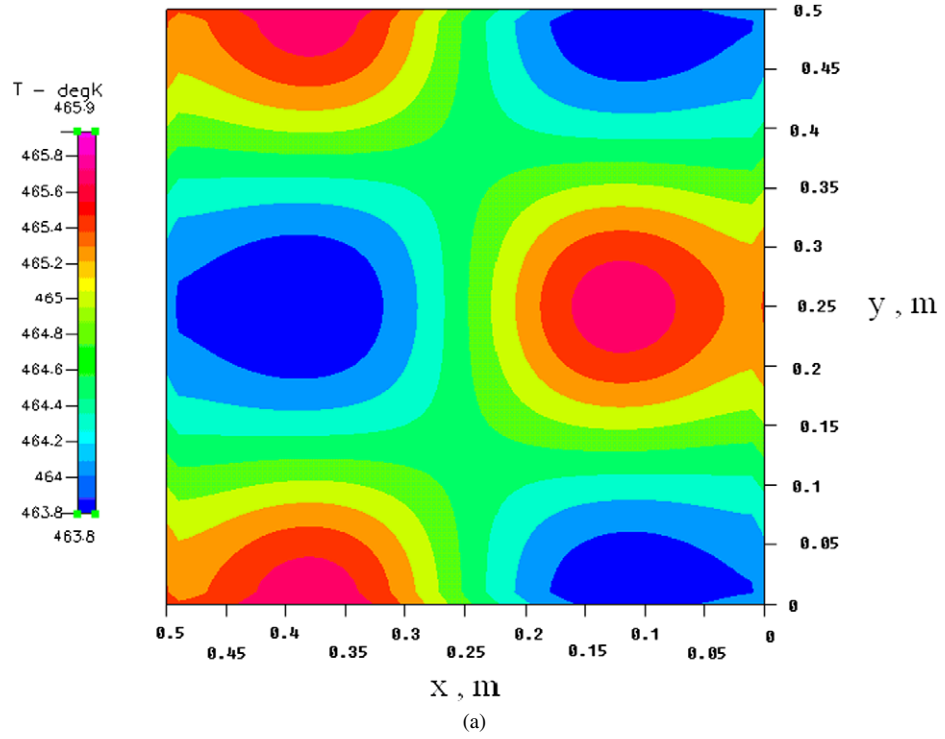

(a)

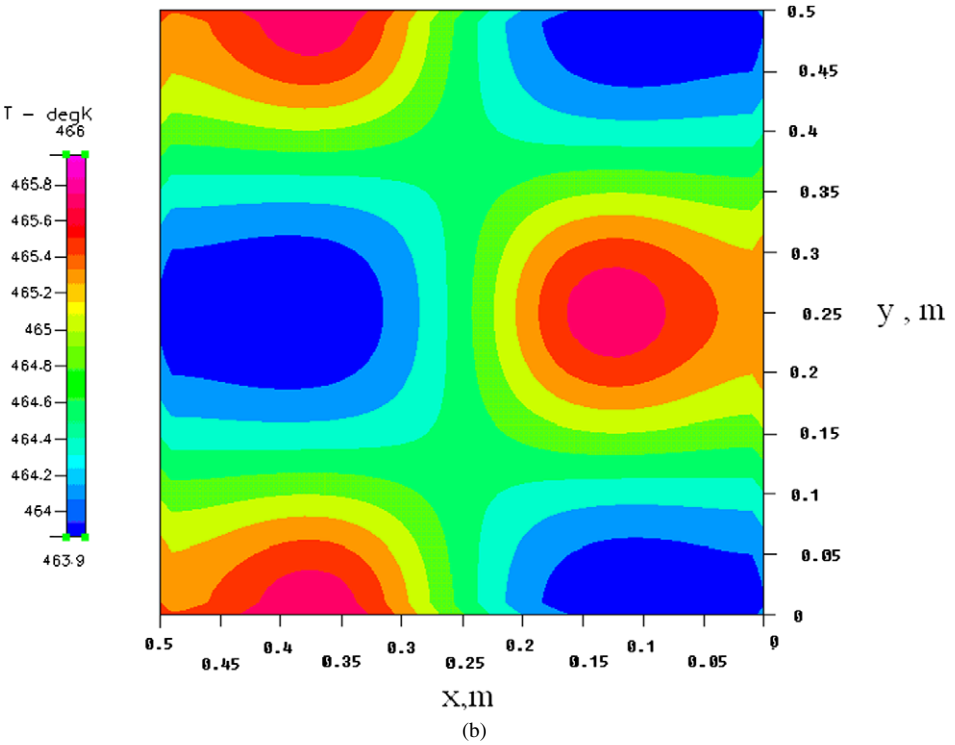

(b)

Fig. 3. The (a) simulated measured and (b) estimated surface temperatures on S_{bottom} with $\sigma = 0.0$ and $f(x, y)^0 = 0.05$ m in case 1.

0.01 m, i.e. there are 51 grid points in both x and y direction. In z direction, 21 grids are always chosen for computations. The boundary condition $T_0 = 200\,^{\circ}\text{C}$ is applied on S_{top}. The measurement surface is always on S_{bottom}, i.e. on the bottom surface.

Three numerical experiments in estimating $f(x, y)$ by the inverse analysis are now presented below:

Numerical test case 1

The unknown surface configuration on S_{top}, $z = f(x, y)$, is assumed as the following form

$$f(x, y) = 0.08 + 0.02 \sin \frac{2\pi x}{0.5} \cos \frac{2\pi y}{0.5} \tag{20}$$

which represents a combination for sine and cosine functions.

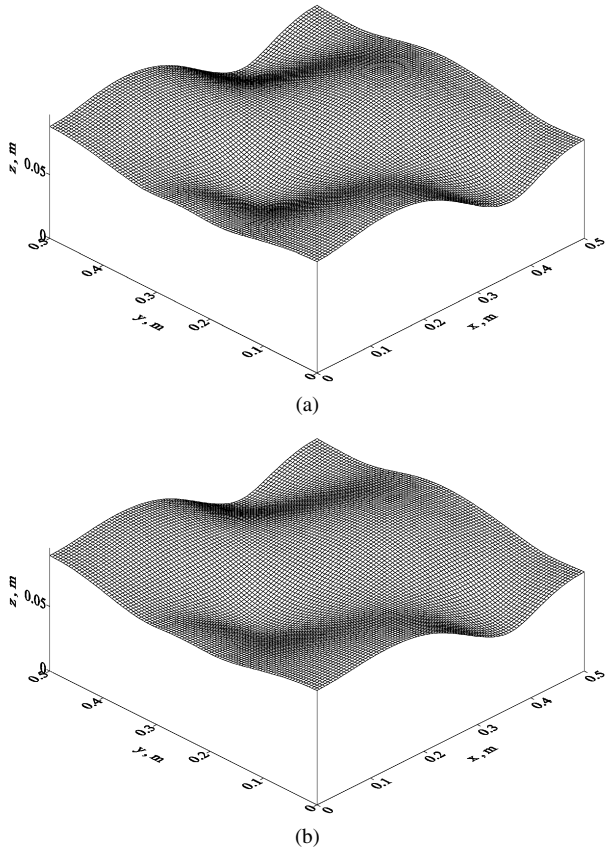

Fig. 4. The estimated surface configurations with $f(x, y)^0 = 0.05$ m in case 1 using (a) $\sigma = 0.11$ and (b) $\sigma = 0.22$.

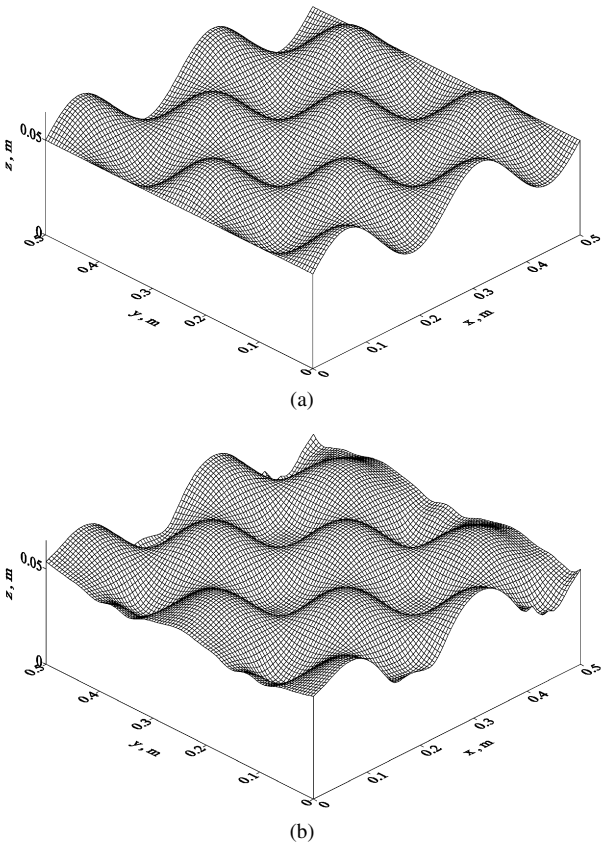

Fig. 6. The (a) exact and (b) estimated surface configurations $f(x, y)$ with $\sigma = 0.0$ and $f(x, y)^0 = 0.05$ m in case 2.

The inverse analysis is first performed by using $q = -5000$ W/m^2 and assuming exact measurements, i.e. $\sigma = 0.0$ and using initial guess $f(x, y)^0 = 0.05$ m with convergent criterion $\varepsilon = 0.2$.

After 26 iterations, the exact and estimated functions of $f(x, y)$ by using CGM are shown in Figs. 2(a) and 2(b), respectively, while the measured and estimated surface temperatures on S_{bottom} are illustrated in Figs. 3(a) and 3(b), respectively.

The average relative errors for the exact and estimated surface configurations and for the measured and estimated temperatures are calculated ERR1 = 1.12% and ERR2 = 0.0014%,

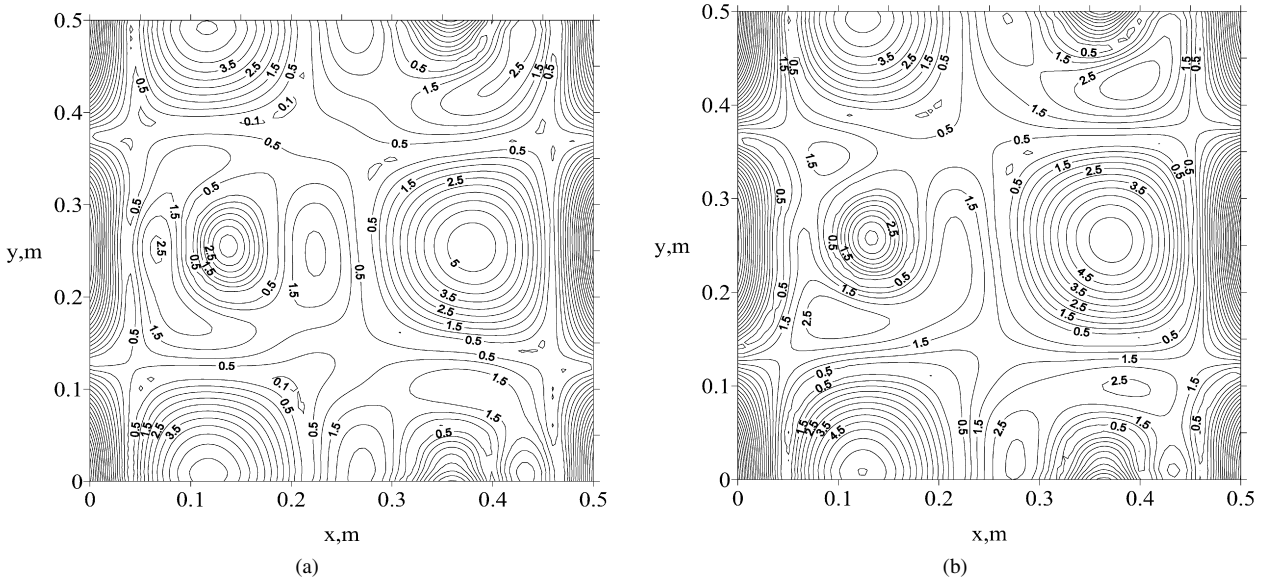

Fig. 5. The contour plots of relative error ERR1 for the estimated surface configurations in case 1 using (a) $\sigma = 0.11$ and (b) $\sigma = 0.22$.

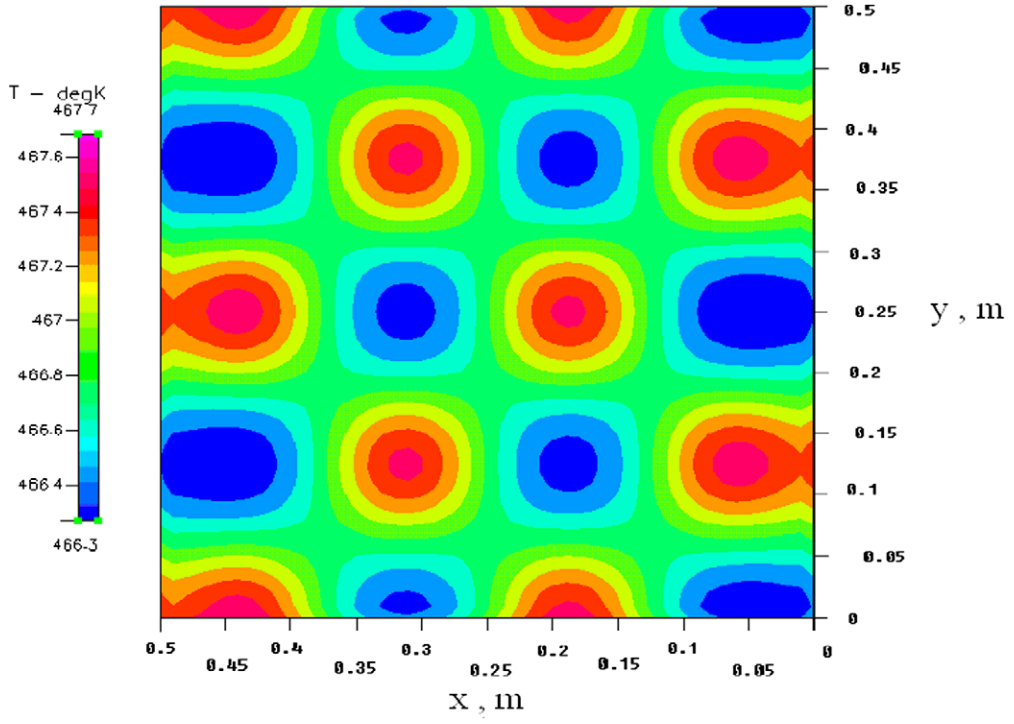

(a)

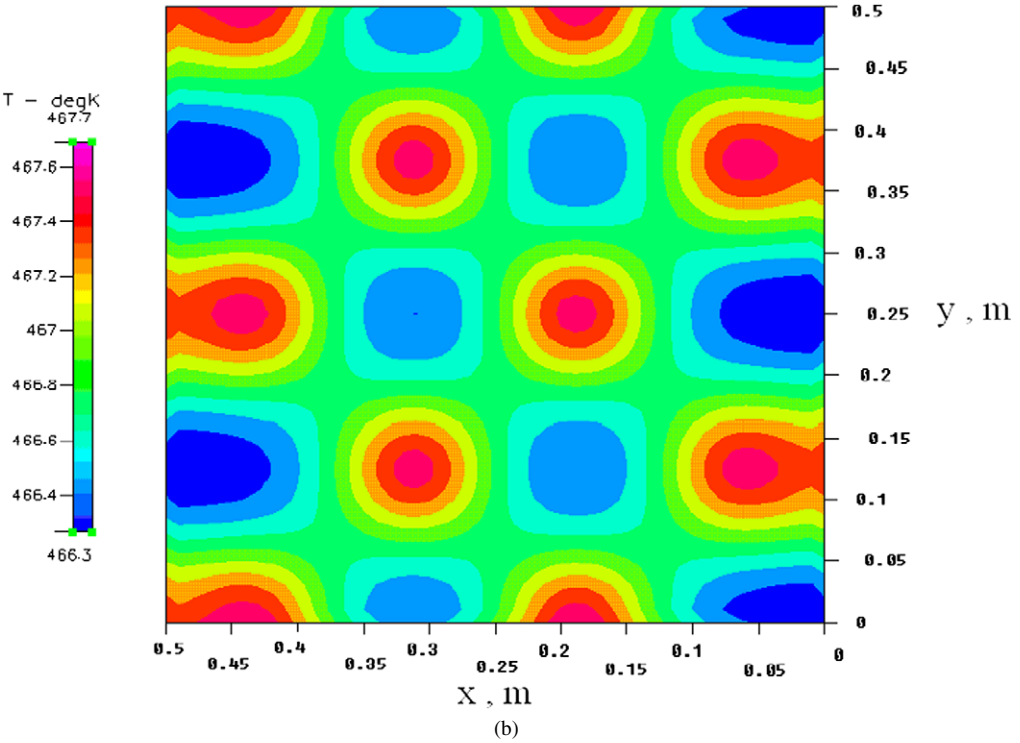

(b)

Fig. 7. The (a) simulated measured and (b) estimated surface temperatures on S_{bottom} with $\sigma = 0.0$ and $f(x, y)^0 = 0.05$ m in case 2.

respectively, where the average relative errors ERR1 and ERR2 are defined as

$$\text{ERR2} = \sum_{n=1}^{N}\sum_{m=1}^{M}\left|\frac{f(x_n, y_m) - \hat{f}(x_n, y_m)}{f(x_n, y_m)}\right| \div (N \times M) \times 100\% \tag{21a}$$

$$\text{ERR2} = \sum_{n=1}^{N}\sum_{m=1}^{M}\left|\frac{T(x_n, y_m) - Y(x_n, y_m)}{Y(x_n, y_m)}\right| \div (N \times M) \times 100\% \tag{21b}$$

here $N = 51$ and $M = 51$ represent the total discreted number of grid in x and y directions, respectively, and $(N \times M)$ indicates the total number of the unknown parameters, while f and

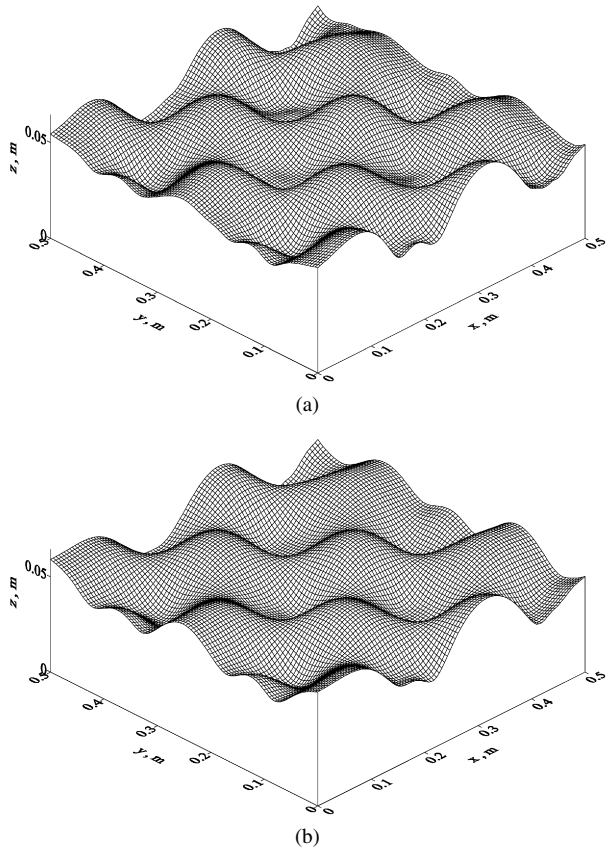

Fig. 8. The estimated surface configurations with $f(x, y)^0 = 0.05$ m in case 2 using (a) $\sigma = 0.07$ and (b) $\sigma = 0.14$.

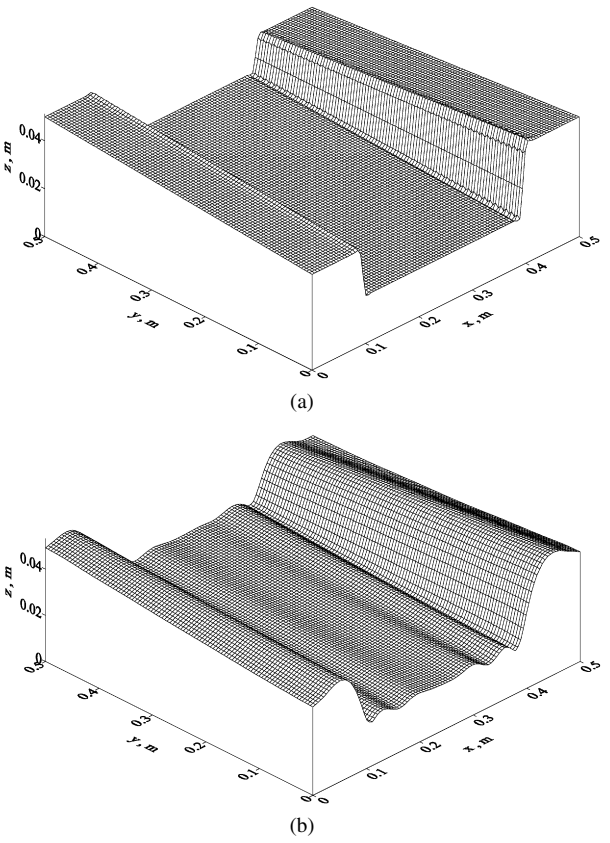

Fig. 9. The (a) exact and (b) estimated surface configurations $f(x, y)$ with $\sigma = 0.0$ and $f(x, y)^0 = 0.05$ m in case 3.

$\hat{f}$ denote the exact and estimated values of surface configurations.

It can be seen from the above figures and relative average errors that the present inverse scheme obtained good estimation for $f(x, y)$ and the CPU time on Pentium IV-3 GHz PC is about 1 hour and 22 minutes.

Next, let us examine what will happen when different initial guess is considered. The computational situations are the same as the previous one except that the initial guess is now chosen as $f(x, y)^0 = 0.15$ m. Using stopping criterion $\varepsilon = 0.2$, after 25 iterations the inverse solutions for the estimated surface shapes and estimated temperatures are obtained and the relative average errors ERR1 and ERR2 are calculated as ERR1 = 1.12% and ERR2 = 0.0013%, respectively. The results are similar to those with $f(x, y)^0 = 0.05$ m. The CPU time (on Pentium IV-3.00 GHz PC) used in the CGM is about 1 hour and 17 minutes. Again, it is clear from the relative average errors that the estimated $f(x, y)$ is still very accurate when using different initial guess for surface shapes.

Finally, let us discuss the influence of the measurement errors on the inverse solutions. The largest temperature difference between all measured temperatures is about 2 °C in the present test case, therefore too large measurement error will be out of its physical significant. For this reason the inclusion of the measurement error will depend on the largest temperature difference on S_{bottom} in the error analysis examples.

First, the measurement error for the simulated temperatures measured by infrared scanners on bottom surface S_{bottom} is taken as $\sigma = 0.11$ (about 5% of the largest temperature difference on S_{bottom}). The estimations for $f(x, y)$ can be obtained after only 13 iterations (CPU time is about 40 minutes) and plotted in Fig. 4(a). The relative average errors ERR1 and ERR2 are calculated as ERR1 = 1.61% and ERR2 = 0.0182%, respectively. The measurement error for the temperatures is then increased to $\sigma = 0.22$ (about 10% of the largest temperature difference on S_{bottom}). After only 7 iterations (CPU time is about 21 minutes) the estimated $f(x, y)$ is obtained and illustrated in Fig. 4(b). ERR1 and ERR2 are calculated as 2.09% and 0.0362%, respectively.

In order to have a better view for the relative error, ERR1, the contour plots based on ERR1 for $\sigma = 0.11$ and $\sigma = 0.22$ are shown in Figs. 5(a) and 5(b), respectively. From Fig. 5 we learn that the estimations along $x = 0$ and 0.5 m are less accurate than the others, it is because that the exact shapes along $x = 0$ and 0.5 m are both straight lines and it is more difficult to reconstruct them. Based on those results it is learned that the reliable inverse solutions can still be obtained when large measurement errors are considered.

Numerical test case 2

In the second test case, $f(x, y)$ is taken as

$$f(x, y) = 0.05 + 0.015 \sin \frac{2\pi x}{0.25} \cos \frac{2\pi y}{0.25} \tag{22}$$

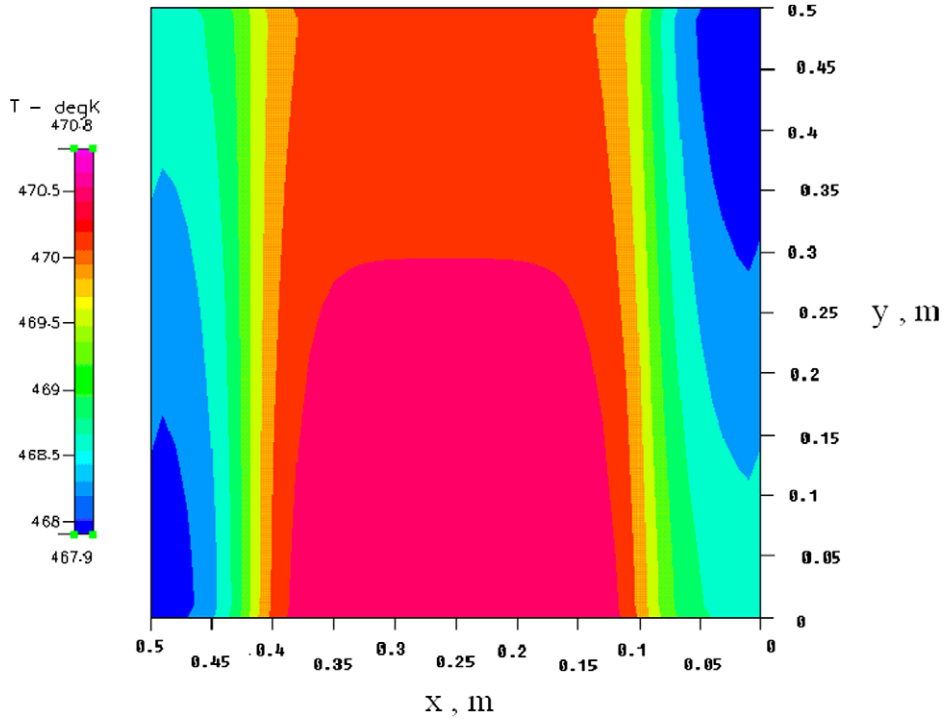

(a)

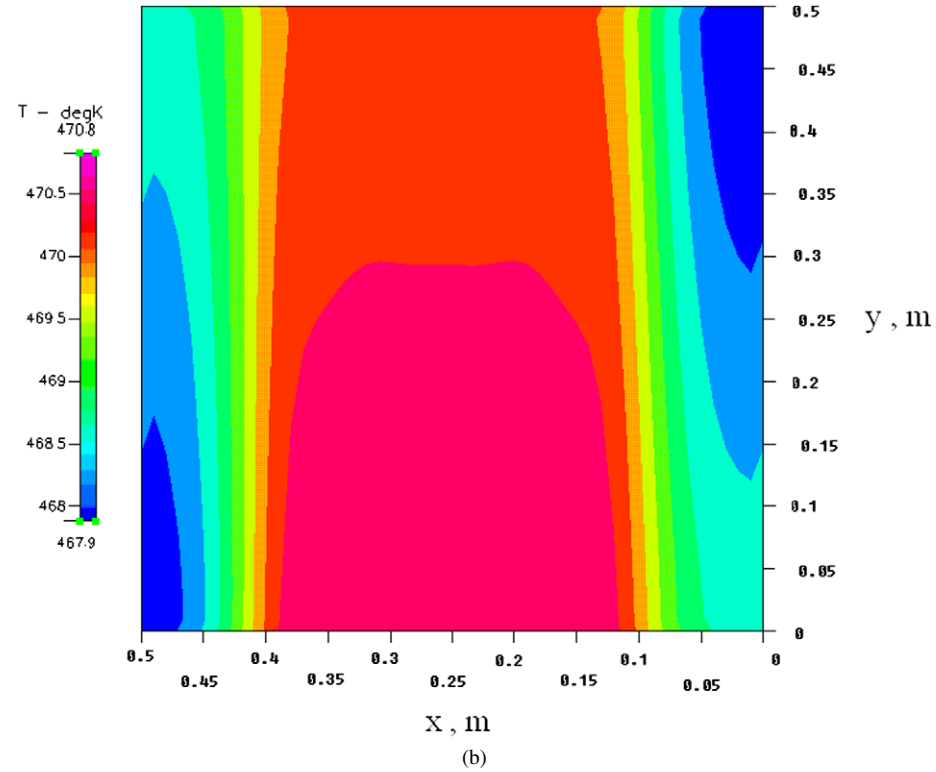

(b)

Fig. 10. The (a) simulated measured and (b) estimated surface temperatures on S_{bottom} with $\sigma = 0.0$ and $f(x, y)^0 = 0.05$ m in case 3.

Eq. (22) still represents a combination for sine and cosine functions but with more fluctuations. The initial guess for this test case is chosen as $f(x, y)^0 = 0.05$ m.

By using $q = -6000$, measurement error $\sigma = 0.0$ and stopping criterion $\varepsilon = 1.34$, after 57 iterations, the exact and estimated functions of $f(x, y)$ are shown in Figs. 6(a) and 6(b), respectively, while the measured and estimated surface temperatures on S_{bottom} are illustrated in Figs. 7(a) and 7(b), respectively. The average relative errors are calculated ERR1 = 1.75% and ERR2 = 0.0036%, respectively.

The estimation for $f(x, y)$ along the boundaries $x = 0$ and $y = 0$ exist some oscillatory behaviors, but the estimated tem-

peratures are still match very well with the measured temperatures on S_{bottom}. It is obvious from Figs. (6) and (7) and the relative average errors that CGM can be used to obtain good estimation for $f(x, y)$ and the CPU time (on Pentium IV-3.00 GHz PC) used in the CGM is about 2 hours and 33 minutes.

Next, error measurement will be considered in the numerical experiments. First, the measurement error for the simulated temperatures measured by infrared scanners on the bottom surface S_{bottom} is taken as $\sigma = 0.07$ (about 5% of the largest temperature difference on S_{bottom}). After 34 iterations (CPU time is about 1 hour and 32 minutes), the estimated $f(x, y)$ can be obtained and shown in Fig. 8(a). The relative average errors ERR1 and ERR2 are calculated as ERR1 = 2.46% and ERR2 = 0.0115%, respectively. Then, the measurement error for the temperatures is increased to $\sigma = 0.14$ (about 10% of the largest temperature difference on S_{bottom}). The estimated $f(x, y)$ can be obtained after only 14 iterations (CPU time is about 39 minutes) and plotted in Fig. 8(b). ERR1 and ERR2 are calculated as 3.28% and 0.0232%, respectively. From Figs. 8(a) and 8(b) we concluded that the reliable inverse solutions can still be obtained when large measurement errors are considered.

Numerical test case 3

In the third test case, a stricter test case for $f(x, y)$ is taken as a step function, i.e.

$$f(x, y) = \begin{cases} 0.04 + 0.02y; & 0 \leqslant x < 0.1 \\ 0.02 + 0.01y; & 0.1 \leqslant x < 0.4 \\ 0.05 - 0.02y; & 0.4 \leqslant x \leqslant 0.5 \end{cases} \tag{23}$$

where the initial guess for this test case is chosen as $z = f(x, y)^0 = 0.02$ m.

By using $q = -5000$, $\sigma = 0.0$ and $\varepsilon = 1.71$, after only 19 iterations, the exact and estimated functions of $f(x, y)$ are shown in Figs. 9(a) and 9(b), respectively. The measured and estimated surface temperatures on S_{bottom} are illustrated in Figs. 10(a) and 10(b), respectively. The average relative errors are calculated ERR1 = 4.98% and ERR2 = 0.0042%, respectively.

The estimated surface shape is not so accurate near the discontinuity region, but the estimated temperatures are still match very well with the measured temperatures on S_{bottom}. Based on Figs. 9 and 10 it is concluded that CGM can be used to obtain good estimation for $f(x, y)$ and the CPU time (on Pentium IV-3.00 GHz PC) used in the CGM is about 48 minutes.

Next, measurement errors will be considered in the numerical experiments. First the measurement error is taken as $\sigma = 0.15$ (about 5% of the largest temperature difference on S_{bottom}). After only 6 iterations (CPU time is about 14 minutes), the estimated $f(x, y)$ can be obtained and shown in Fig. 11(a). The relative average errors ERR1 and ERR2 are calculated as ERR1 = 7.03% and ERR2 = 0.0236%, respectively. The measurement error for the temperatures is then increased to $\sigma = 0.3$ (about 10% of the largest temperature difference on S_{bottom}). The estimated $f(x, y)$ can be obtained after only 3 iterations (CPU time is about 8 minutes) and plotted in Fig. 11(b). ERR1 and ERR2 are calculated as 7.81% and 0.0465%, respectively. From Figs. 11(a) and 11(b) it is concluded that the reliable inverse solutions can still be obtained when large measurement errors are considered.

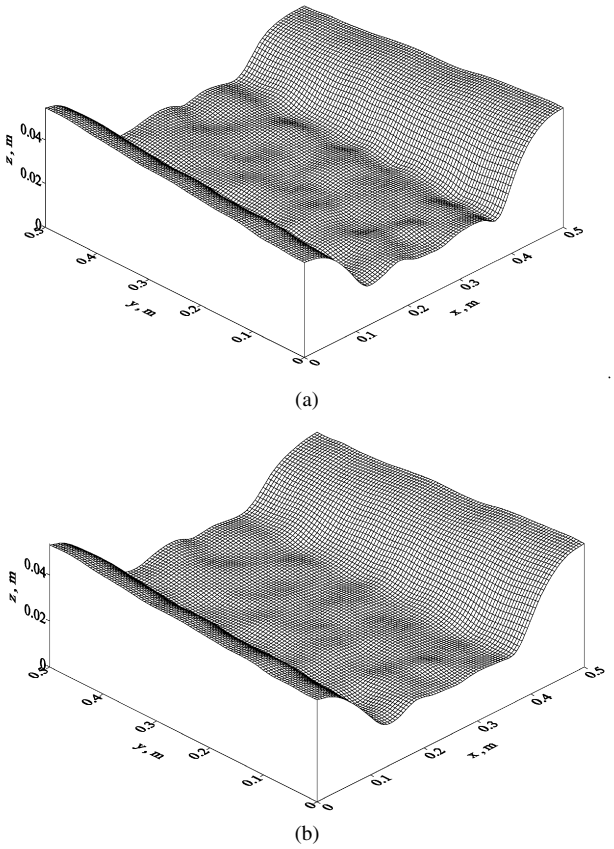

Fig. 11. The estimated surface configurations with $f(x, y)^0 = 0.05$ m in case 3 using (a) $\sigma = 0.15$ and (b) $\sigma = 0.3$.

From the above numerical test cases 1, 2 and 3, we concluded that the advantages of the CGM in estimating unknown surface configurations lie in that (i) it does not require a very accurate initial guess and (ii) the rate of convergence is fast.

10. Conclusions

The Conjugate Gradient Method (CGM) with commercial code CFD-RC are successfully applied for the solution of the three-dimensional inverse geometry problem in determining the unknown irregular surface configuration by utilizing surface temperature measurements. Several test cases involving different initial guess, functional forms of $f(x, y)$ and measurement errors were considered. The results show that CGM does not require an accurate initial guess of the unknown quantities and needs very few numbers of iterations in performing the inverse calculations on Pentium IV-30 GHz PC.

Acknowledgement

This work was supported in part through the National Science Council, R. O. C., Grant number, NSC-95-2221-E-006-469.

References

[1] O.M. Alifanov, Solution of an inverse problem of heat conduction by iteration methods, J. Engrg. Phys. 26 (1972) 471–476.

[2] C.H. Huang, J.Y. Yan, An inverse problem in simultaneously measuring temperature dependent thermal conductivity and heat capacity, Int. J. Heat Mass Transfer 38 (1995) 3433–3441.

[3] C.H. Huang, C.Y. Yeh, Helcio R.B. Orlande, A non-linear inverse problem in simultaneously estimating the heat and mass production rates for a chemically reacting fluid, Chem. Eng. Sci. 58 (16) (2003) 3741–3752 (SCI&EI paper).

[4] A.J. Kassab, J. Pollard, A cubic spline anchored grid pattern algorithm for high resolution detection of subsurface cavities by the IR-CAT method, Numer. Heat Transfer, Part B 26 (1994) 63–78.

[5] G.S. Dulikravich, T.J. Martin, Inverse design of super-elliptic cooling passages in coated turbine blade airfoil, J. Thermophys. Heat Transfer 8 (1994) 288–294.

[6] A.J. Kassab, C.K. Hsieh, J. Pollard, Solution of the inverse geometric problem for the detection of subsurface cavities by the IR-CAT method, in: L.C. Wrobel, D.B. Ingham (Eds.), Boundary Integral Formulations for Inverse Analysis, Computational Mechanics Publications, Boston, 1997 (Chapter 2).

[7] C.K. Hsieh, A.J. Kassab, A general method for the solution of inverse heat conduction problems with partially unknown system geometries, Int. J. Heat Mass Transfer 29 (1) (1985) 47–58.

[8] T. Burczynski, W. Beluch, A. Dlugosz, W. Kus, M. Nowakowski, P. Orantek, Evolutionary computation in optimization and identification, Comput. Assist. Mech. Eng. Sci. 9 (1) (2002) 3–20.

[9] T. Burczinski, J.H. Kane, C. Balakrishna, Shape design sensitivity analysis via material derivative-adjoint variable technique for 3D and 2D curved boundary elements, Int. J. Numer. Meth. Eng. 38 (1995) 2839–2866.

[10] C.H. Cheng, C.Y. Wu, An approach combining body-fitted grid generation and conjugate gradient methods for shape design in heat conduction problems, Numer. Heat Transfer B 37 (2000) 69–83.

[11] C.H. Huang, B.H. Chao, An inverse geometry problem in identifying irregular boundary configurations, Int. J. Heat Mass Transfer 40 (9) (1997) 2045–2053.

[12] C.H. Huang, C.C. Tsai, A transient inverse two-dimensional geometry problem in estimating time-dependent irregular boundary configurations, Int. J. Heat Mass Transfer 41 (12) (1998) 1707–1718, NSC-87-2212-E-006-107.

[13] C.H. Huang, C.C. Chiang, H.M. Chen, Shape identification problem in estimating the geometry of multiple cavities, AIAA, J. Thermophys. Heat Transfer 12 (2) (April–June 1998) 270–277.

[14] C.H. Huang, H.M. Chen, An inverse geometry problem of identifying growth of boundary shapes in a multiple region domain, Numer. Heat Transfer, Part A 35 (1999) 435–450.

[15] C.H. Huang, C.C. Shih, A shape identification problem in estimating simultaneously two interfacial configurations in a multiple region domain, Appl. Thermal Engrg. 26 (1) (2006) 77–88.

[16] E. Divo, A.J. Kassab, F. Rodriguez, An efficient singular superposition technique for cavity detection and shape optimization, Numerical Heat Transfer, Part B 46 (2004) 1–30.

[17] CFD-RC user's manual, ESI-CFD Inc. 2005.

[18] L.S. Lasdon, S.K. Mitter, A.D. Warren, The conjugate gradient method for optimal control problem, IEEE Trans. Automatic Control AC-12 (1967) 132–138.

[19] IMSL Library Edition 10.0, User's Manual: Math Library Version 1.0, IMSL, Houston, TX, 1987.